(Received 20 February 2025, Accepted 14 April 2025, Scheduled 26 April 2025)

Revealing the Spatial Distribution of Radiation Emitted by Simple Objects

Edmund K. Miller*

Los Alamos National Laboratory (retired), Lincoln, USA

ABSTRACT: This article summarizes the author's work over the years having the goal of developing computational tools for determining the quantitative distribution of where radiation is emitted from objects of interest.

1. BACKGROUND

The capability to determine quantitatively the radiation and scattering properties of conducting and penetrable objects of increasing complexity as a function of time and frequency is now well established. It is also true that the fundamental cause of electromagnetic (EM) radiation is charge acceleration. This knowledge has long been exploited in the physics community in connection with such applications as the design of particle accelerators and radio astronomy. Radio telescopes have become indispensable tools in the tremendous strides that have been made over the last century in revealing the cosmological origins of the universe.

But where such EM radiation originates came up periodically over time without any satisfactory answer. A colleague Dr. Jeremy Landt and I published an invited article in the IEEE Proceedings on "Direct Time-Domain Techniques for Radiation and Scattering from Wires" in 1980 [1]. One of the topics we discussed was the propagation of current and charge pulses down the arms of a wire dipole antenna. We included results that showed the attenuation of these pulses with distance and referred to them privately as a "radiation droop" without any further evidence to support this observation, but it did turn out to be the explanation.

I periodically revisited this issue, and in the 1996 of my column "PCs for AP and Other EM Reflections" in the IEEE Antennas and Propagation Society (APS) Magazine I revisited the sinusoidal current filament (SCF) [3, 4]. In particular I used the Induced EMF Method to compute the equivalent input power as a function of position along the SCF, which I could not recall ever having seen previously. This was interesting in that a plot of this result revealed a lobed pattern along the length of the current filament. Since the SCF is a standing wave and there is zero net power flow along it, this result seemed to indicate that its length-wise radiated power would have that same structure too.

One question this raised was could where the radiated far-field power be determined to confirm this? The SCF far field can be expressed in a closed form that seems to indicate that the radiated power at most comes only from the feedpoint and ends of the filament depending on its length. How is this apparent difference to be reconciled? A paper by Jackson [2] that had recently come to my attention initially seemed to have something to offer concerning the spatial power radiation from a dipole current. The opening sentence of this paper somewhat dashed this expectation: "This paper is a didactic discussion of how the EM energy radiated by an antenna emerges from a localized source, is guided by the antenna's conductors, and ultimately **shakes** (my emphasis) free to form the radiation described by the asymptotic Poynting vector." Jackson devoted the rest of the article to Poynting Vector streamlines and did not provide any further clarification of how "shakes free" relates to charge acceleration.

2. DEVELOPMENT OF FARS

2.1. FARS Results for a Sinusoidal Current Filament

In the meantime, I developed a procedure called Far-field Analysis of Radiation Sources (FARS) as a trial attempt to determine the quantitative distribution of where radiation occurs from the SCF. This procedure handled the computation order of the radiated power different from the usual approach. Still, it yields an identical result for the total radiated power and was first reported in my APS column in 1999 [4]. Further details of frequency-domain Frequency-Domain FARS (FD-FARS) in Numerical Electromagnetics Code (NEC) and time domain Time-Domain FARS (TDFARS) in Thin-Wire Time Domain (TWTD) can be found in [4, 5]. Both NEC and TWTD are integral-equation models with NEC using a 3-term constant, sine and cosine basis function while TWTD uses a 9-term space-time quadratic basis, and both employ delta-function weights and point testing.

When I compared the IEMF and FARS results for the SCF, their agreement was within a percent or so! A representative

* Corresponding author: Edmund K. Miller (e.miller@ieee.org).

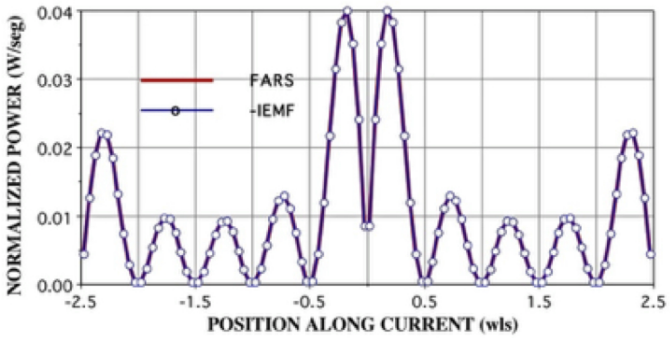

FIGURE 1. A comparison of FARS and IEMF for a 5 wavelength SCF.

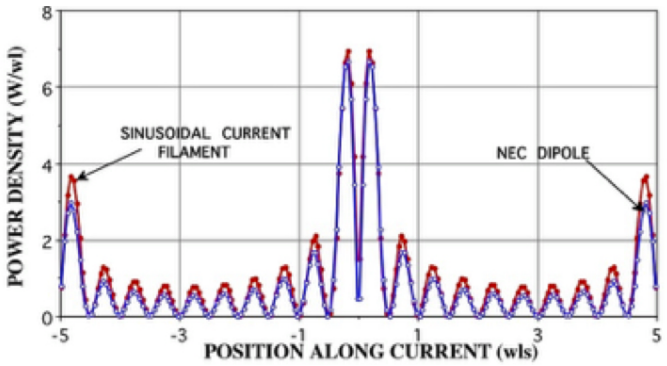

FIGURE 2. The SCF and NEC power densities for a 10-wavelength current filament and wire.

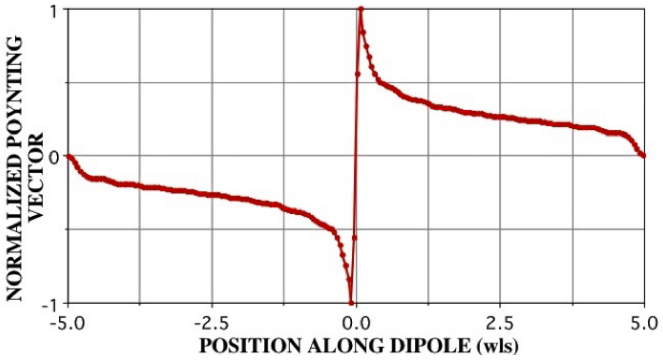

FIGURE 3. The on-surface Poynting vector for the NEC dipole.

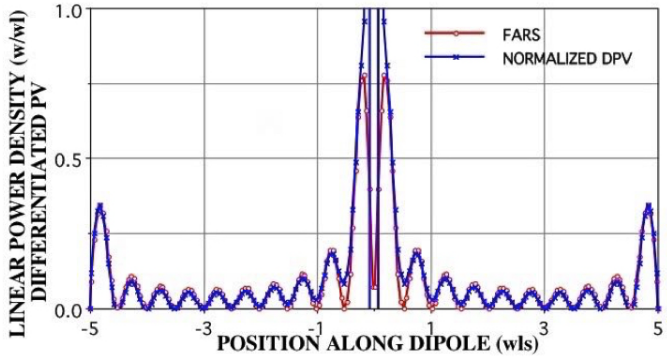

FIGURE 4. The FARS and DPV results for the NEC dipole.

result of their comparison is shown in Fig. 1. Observe that the IEMF result portrays the input power which is opposite in sign from the radiated power, and its negative value is shown here. Additional examples of these kinds of results can be found in [5] for various lengths that exhibit similar agreement between IEMF and FARS.

2.2. Comparing FARS for a SCF and NEC Dipole

The next test for FARS was the boundary-value problem of a thin-wire dipole antenna modeled using NEC. A result for a 10-wavelength SCF and a dipole 1 mm in diameter, each having a maximum current of 1 A, is shown in Fig. 2. The results are very close but with the SCF power density slightly higher due to the attenuation of the NEC current along the dipole. These results are presented for longer currents to display length effects more clearly.

2.3. Charge Acceleration on a Wire Away from the Feedpoint

While it can be concluded that the FARS results for the SCF imply an associated charge acceleration due to the IEMF input power, what accounts for a similar radiated power for the NEC dipole. Examining the on-surface, tangential Poynting vector (PV) helps clarify the situation as shown in Fig. 3 for the same 10-wavelength dipole. The power flow down the two arms of the dipole appears decreasing monotonically. The only plausible explanation for this would seem to be that the outward-propagating power flow decreases due to radiation, as shown by FARS in Fig. 2.

The differentiated PV (DPV) of Fig. 3, normalized to the FARS result, is plotted for the NEC dipole in Fig. 4. The FARS results agree to the DPV result within a few percent except at the feedpoint, confirming the conjecture that the radiated power accounts for the attenuated PV on the dipole. This indicates that charge acceleration is involved in the power loss, which raises the question of what is causing charge acceleration to occur where there is no excitation? For an answer we will turn next to the time domain.

3. CHARGE ACCELERATION IN THE TIME DOMAIN

Time-domain results offer a complementary and generally more natural way to explore charge acceleration, which is, of course, a time-related phenomenon. The results that follow were obtained using the TWTD code [6]. The graph in Fig. 5 displays the current and charge density times the light speed at several time steps for a long wire excited at its center by a Gaussian voltage pulse. The outward propagating current is positive on both halves while the charge pulses are of opposite sign. This is because the applied voltage pulse accelerates a positive charge to the right and a negative charge to the left.

More significantly, the amplitudes of the current and change pulses decrease with distance traveled. This is due to their partial reflection as they propagate. Integrating successive charge

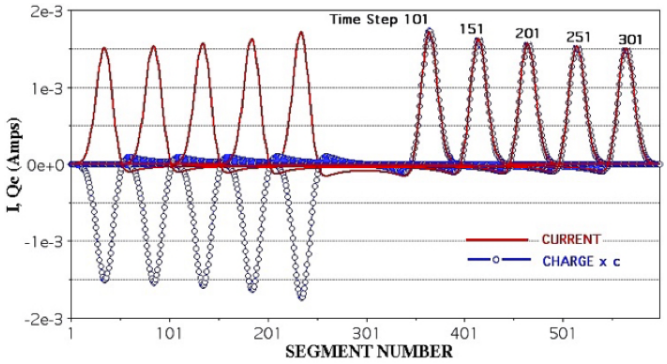

FIGURE 5. Current and charge pulses on dipole antenna.

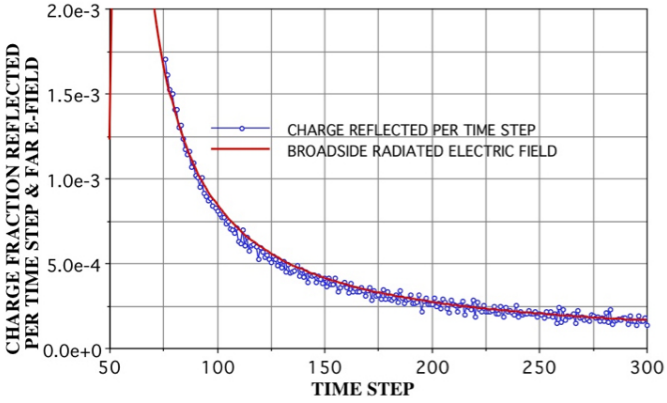

FIGURE 6. Charge reflected per time step and the broadside radiated electric field.

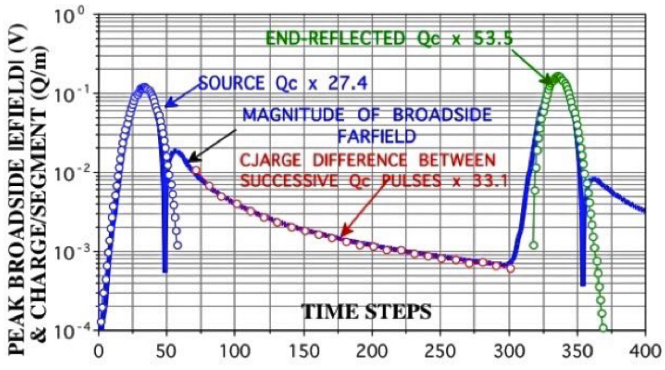

FIGURE 7. Broadside radiated electric field time variation and associated charge magnitudes.

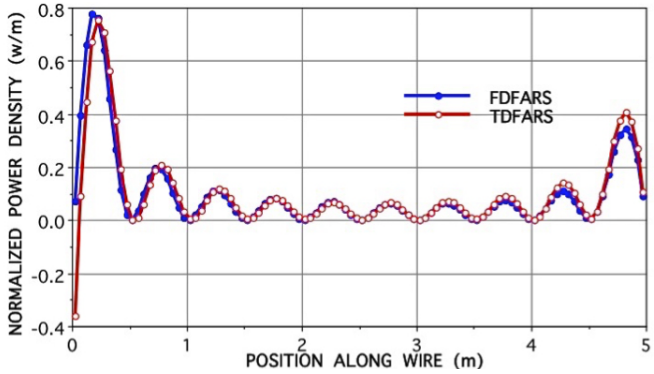

FIGURE 8. Comparison of FDFARS and TDFARS for time-harmonic excitation.

pulses and taking their difference yields the charge loss per time step, as shown in Fig. 6. Also plotted there is the time-dependent broadside radiated electric field. Their time variation is essentially graphically indistinguishable aside from the numerical noise" due to subtracting only slightly different quantities of change from step to step.

This result provides strong evidence that the effect of a change in charge velocity of 2c, i.e., acceleration, is the cause of the radiated electric field. The results of Fig. 7 provide a more complete view of the radiation due to the initial pulse caused by the feedpoint voltage, the end-reflection radiation, and the intermediate charge reflection.

An advantage of the time separation of a time-domain solution is to make it possible to associate source and field effects. The multipliers on the graph are proportionality or acceleration factors (AFs) to relate the charge quantity to its associated field value. Observe that the AF for the source is about half that of the end reflection value. This is reasonable since the speed or velocity change is c at the source and 2c at the end reflection. The propagation-reflection AF is also smaller than that for the end reflection radiation, probably because their reflection mechanisms vary physically.

There is another perspective from which to explore time-domain radiation.

4. COMPARISON OF FDFARS AND TDFARS

After finding the usefulness of FDFARS in NEC, it was a natural step to add TDFARS to TWTD. As one of the first checks on its validity a dipole having the same dimensions and numerical model as used for NEC was run and as an excitation a step Gaussian pulse envelop and with the frequency variation used for one of the FDFARS runs. The time duration of the TWTD model was run until a steady state was reached. The normalized results are presented in Fig. 8 for the right half of the dipole.

The two results agree within 1 percent or so except at the feedpoint and end whose cause is not obvious. One possibility is that NEC and TWTD necessarily use different basis functions. However, the agreement demonstrated between these two very different models is considered acceptable as a check on both TDFARS and FDFARS.

It is interesting to compare the two FARS results for time-harmonic and impulse excitation, as shown in Figs. 9 and 10. The total power and energy are 1 W and 1 J, respectively, so the area under each curve is unity.

The most significant difference between the above time- and frequency-domain FARS results is the monotonic spatial variation of the former and the lobed variation of the latter due to its standing-wave behavior. This demonstrates the physical insight the FARS analysis provides.

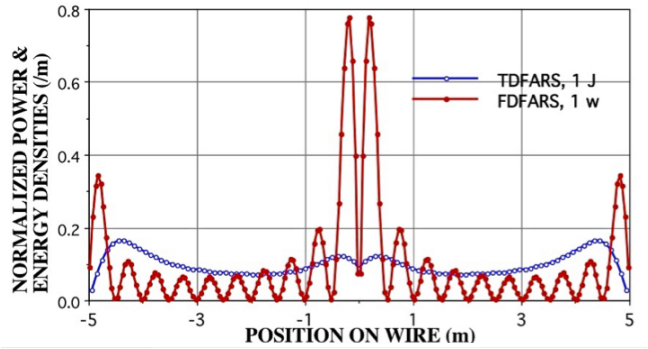

FIGURE 9. Center-excited dipole 10 m long.

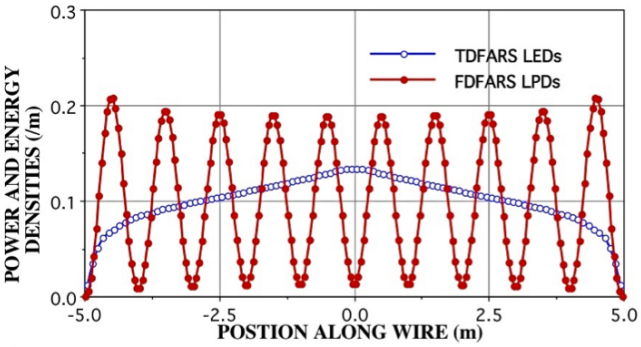

FIGURE 10. Normal-incidence plane wave of 10-m wire.

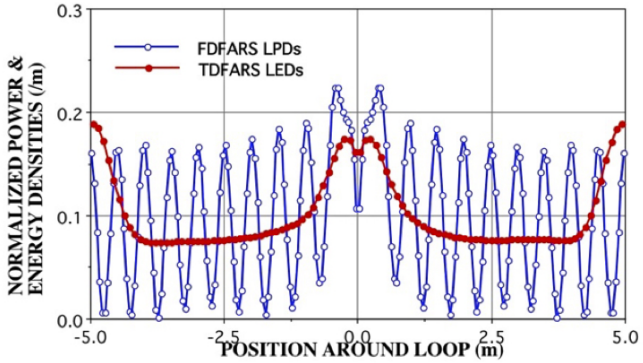

FIGURE 11. Normalized time- and frequency-domain FARS for a circular loop.

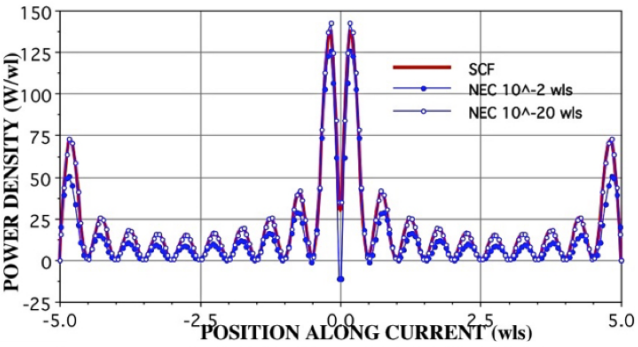

FIGURE 12. FDFARS for 10-wavelength SCF & NEC dipoles 10^{-3} and 10^{-20} wavlengths.

Continuing the time- and frequency-domain normalized FARS comparisons, a result for a circular loop is shown in Fig. 11 with the feedpoint at 0 in these plots. The TDFARS version has maxima opposite the feedpoint, which it also exceeds in value. This effect on the circular loop is caused when opposite-signed charge pulses meet there. Their reflection radiation is additive and becomes spatially coherent over the far-field sphere thus doubling that from the feedpoint.

5. SOME ADDITIONAL FARS EXAMPLES

A sampling of various other situations to demonstrate further features of FARS will conclude this discussion. Since the motivation for developing FARS originated from an investigation of radiation from an SCF, it was interesting to see whether an NEC dipole whose wire radius approached zero might compare with the SCF. Recall that the SCF served as a surrogate for a thin-wire antenna before the evolution of CEM. The FARS plots in Fig. 12 are for a 10-wavelength SCF and NEC dipoles having radii of 10^{-3} and 10^{-20} wavelengths. A plot of the NEC dipole radiated power versus its radius is shown in Fig. 13.

The above NEC and SCF results are for a maximum current of 1 A. At the smallest radius shown in Fig. 13, the NEC radiated power is within 0.5% of that for the SCF. FDFARS plots for a 10-wavelength dipole with bends of different angles 3 wavelengths from its center are shown in Fig. 14.

The bends exhibit the charge acceleration they cause and an associated increased local radiated power that somewhat resembles the feedpoint variation. It is worth noting that for both an NEC dipole and SCF the feedpoint FDFARS results are quite different for lengths that are an even and odd number of half wavelengths as Figs. 12 and 15 demonstrate.

An alternating maximum or minimum of the current at that location causes the feedpoint variation exhibited in Figs. 12 and 15. A maximum occurs for a current length of an odd number of half wavelength while a minimum occurs for an even number.

An FDFARS result for a 5-element NEC-modeled Yagi-Uda array is shown in Fig. 16 for a 1-V exciting source.

The reflector absorbs power which has the effect of reducing the backwards radiation from this array.

6. TIME-DOMAIN ENERGY MEASURES

It has been found helpful in time-domain models to compute an "energy measure" of the time history of their electric and magnetic components [1]. These quantities are obtained by integrating the squared current and charge density times light speed over the object as a function of time. An example of this result is shown in Fig. 17 for a straight wire.

Observe that the current and charge energies are equal during the time their pulses are away from the center feedpoint and the ends. During end reflection, the current energy becomes 0 while the charge energy zeroes as the opposite-sign charges coincide at the feedpoint. More details are available in [5]. Differentiating the total energy, the loss rate due to radiation is obtained, as presented in Fig. 18.

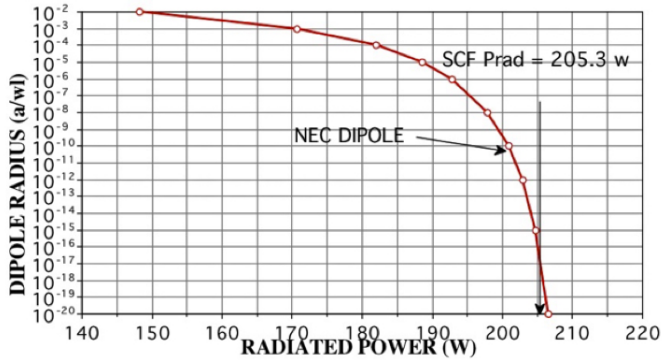

FIGURE 13. NEC dipole radiated power as a function of its radius.

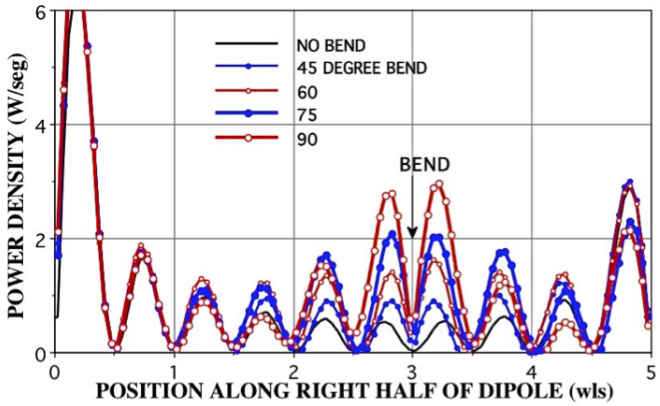

FIGURE 14. FDFARS on the right half of a NEC dipole having various bend.

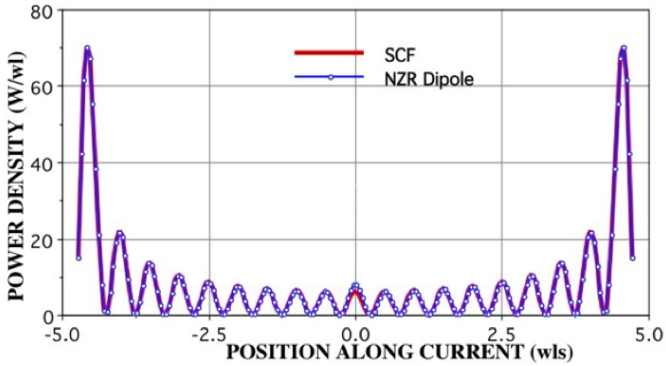

FIGURE 15. FDFARS for 9.5 wavelength NEC dipole and SCF.

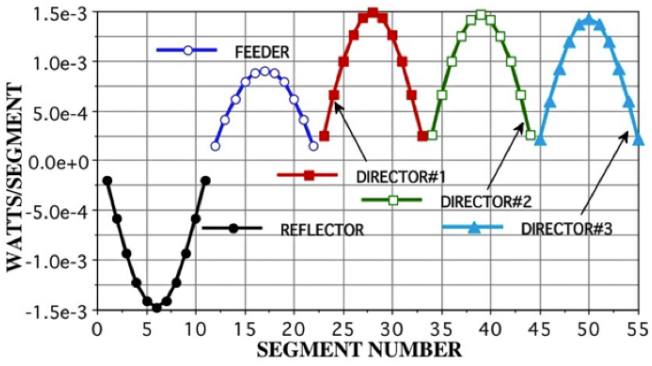

FIGURE 16. Results for a Yagi-Uda array.

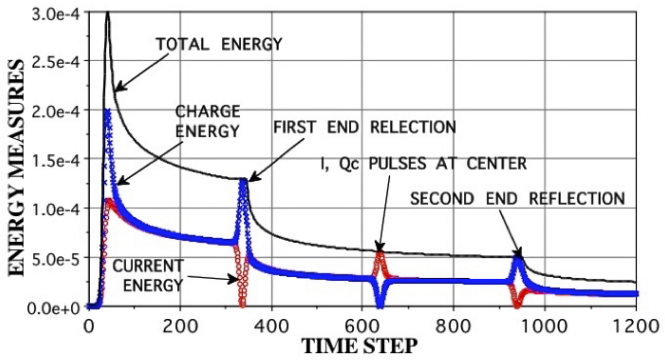

FIGURE 17. The current and charge energies for a 599-segment dipole.

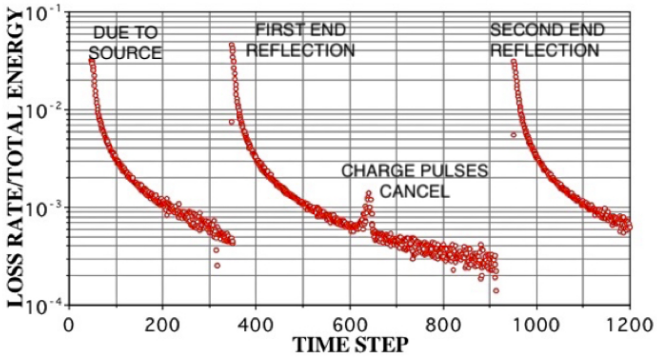

FIGURE 18. Differentiated total energy from Fig. 17.

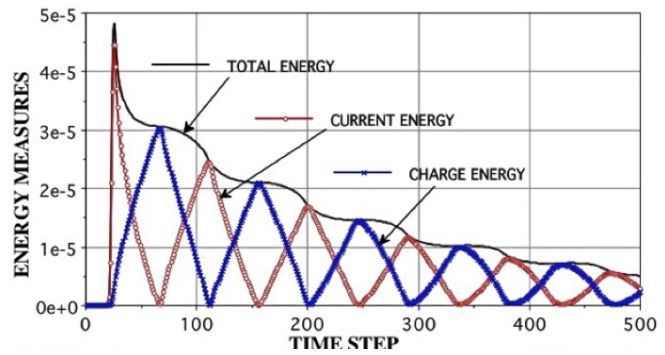

FIGURE 19. Current and charge energies for a 199-segment wire.

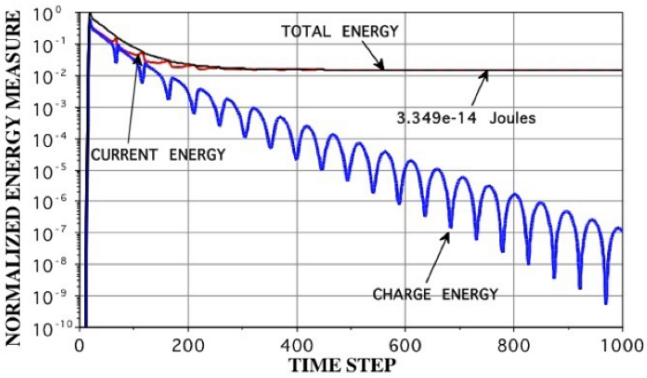

FIGURE 20. Current and charge energies for a 1000-segment loop.

A result like Fig. 17 for a normally incident plane scattering from a 199-segment straight wire is included in Fig. 19.

The energy plot for a 100-segment circular loop is shown in Fig. 20. In this case, the charge energy reaches 0 as a steady-state uniform current is established, and there is no further radiation. It is interesting that TWTD can be used to find the inductance of closed loops of essentially any geometry.

7. CONCLUDING COMMENT

Mathematical details of the results presented here can be found in [5], from which much of this material has been excerpted. The two computational tools, FDFARS and TDFARS, used to get the results presented are simple post-processors that can be readily added to literally any computer code.

ACKNOWLEDGEMENT

The author greatly appreciates the assistance of G. J. Burke in adding FARS to the NEC and TWTD codes and help in their use.

REFERENCES

[1] Miller, E. K. and J. A. Landt, "Direct time-domain techniques for transient radiation and scattering from wires," *Proceedings of the IEEE*, Vol. 68, No. 11, 1396–1423, 1980.

[2] Jackson, J. D., "How an antenna launches its input power into radiation: The pattern of the Poynting vector at and near an antenna," *American Journal of Physics*, Vol. 74, No. 4, 280–288, 2006.

[3] Miller, E. K., "PCs for AP and other EM reflections," *IEEE Antennas and Propagation Magazine*, Vol. 37, 70–74, Oct. 1996.

[4] Miller, E. K., "PCs for AP and other EM reflections," *IEEE Antennas and Propagation Magazine*, Vol. 41, 82–86, Apr. 1999.

[5] Miller, E. K., *Charge Acceleration and the Spatial Distribution of Radiation Emitted by Antennas and Scatterers*, IET Press, 2022.

[6] Landt, J. A., E. K. Miller, and M. V. Blaricum, *WT-MBALLLlB: A Computer Program for the Time Domain Electromagnetic Response of Thin-Wire Structures*, No. 210, AFWL Interactions Notes, Lawrence Livermore Laboratory, 1974.